SANDIA REPORT SAND83−0166 • Unlimited Release • UC−70
Printed June 1983

Petrographic Study of Evaporite Deformation Near the Waste Isolation Pilot Plant (WIPP)

David J. Borns

SAND83-0166

2900-Q(6-82)

Petrographic Study of Evaporite Deformation Near the Waste Isolation Pilot Plant (WIPP)

David J. Borns
Earth Sciences Division 9731
Sandia National Laboratories
Albuquerque, NM 87185

Abstract

The Delaware Basin of southeastern New Mexico contains ~1000 m of layered evaporites. Areas in the northern Delaware Basin, bordering the Capitan reef, have anomalous seismic reflection characteristics, such as loss in reflector continuity. Core from holes within this zone exhibits complex mesoscopic folds and extension structures. On a larger scale, anticlines and synclines are indicated by structure contours based on boreholes. The deformation is probably gravity-driven. Such a process is initiated by basin tilting during either a Mesozoic or Cenozoic period of uplift. The age of deformation is equivocal, ranging from Permian to Recent.

Small-scale structures suggest that deformation was episodic with an early, syndepositional stage of isoclinal folding. Later, open-to-tight asymmetric folding is more penetrative and exhibits a sense of asymmetry opposite to that of the earlier isoclinal folding. The younger folds are associated with development of zonal crenulation cleavage and microboudinage of more competent carbonate layers. At the same time, halite beds developed dimensional fabrics and convolute folds in anhydrite stringers. Late-stage, near-vertical fractures formed in competent anhydrite layers. Microscopic textures exhibit rotated anhydrite porphyroblasts, stress shadow growth, and microboudinage. Except during late-stage deformation, anhydrite and halite recrystallized synkinematically. Drastic strength reduction in anhydrites through dynamic recrystallization occurs experimentally near 200°C. However, evaporites of the WIPP site never experienced temperatures >40°C. Microscopic fabrics and P, T history of the evaporites suggest that pressure solution was the active mechanism during deformation of evaporites at the WIPP site. This conclusion stresses the importance of fluid in facilitating deformation in low-temperature evaporite sequences. The formation of pressurized brine pockets is empirically associated with deformation. The development of high-angle fractures in the uppermost anhydrite unit of the Castile in response to folding provides the reservoir for the brines. Brine fluids may have emanated from deforming halite and anhydrite units through pressure-solution-induced reduction of porosity.

Contents

Figures

Figures (cont)

Tables

Petrographic Study of Evaporite Deformation Near the Waste Isolation Pilot Plant (WIPP)

1. Introduction

The Delaware Basin of southeastern New Mexico contains layered evaporites ~1000 m thick (see Figure 1). An area in the northern part of the basin has been selected as the site for the Waste Isolation Pilot Plant, herein called WIPP. Rock units of interest in this report are largely Ochoan. The oldest unit is the Castile Formation, which primarily consists of three anhydrite units separated by two halite units (see Figure 2). The second oldest is the Salado Formation, which consists of halite, anhydritic, and/or polyhalitic halite. The youngest unit is the Rustler Formation, which contains siltstones, anhydrites, dolomitic siltstones, dolomites and halite.

Evaporite beds are deformed within portions of the Delaware Basin along its margins and in some areas in the middle of the basin (see Figure 3). The term "Disturbed Zone" (DZ) has been used to identify areas with deformation features in the northern part of the WIPP site. This DZ is now delineated based on the evidence of structure exhibited in boreholes and by seismic reflection data (Borns et al, 1983).

The origin of deformation at the WIPP site remains controversial. Kirkland and Anderson (1970) described the occurrence of microfolded anhydrite-calcite laminae in the Castile Formation in Eddy County, New Mexico, and Culberson County, Texas. They related this folding to compressional deformation that accompanied regional tectonism rather than to syndepositional processes. Starting in the mid-1970s, an extensive drilling program was started in the northern Delaware Basin to assist site selection and characterization for a nuclear-waste test facility. The first of these drillholes, ERDA 6, encountered a large-scale anticline and mesoscopic folding, in part complex (Anderson and Powers, 1978; Jones, 1981). Anderson and Powers correlated this deformation to the microfolding observed by Kirkland and Anderson (1970). Subsequent drillholes (WIPP 10, 11, 12, and 13) in the northern portions of the site revealed deformation styles similar to those of ERDA 6.

The origin of these deformation features has been the source of considerable debate. The envisaged possible mechanisms for deformation are as follows:

1. Dissolution (Anderson and Kirkland, 1980)
2. Gypsum dehydration (Kirkland and Anderson, 1970).
3. Halokinesis (Trusheim, 1960; Borns et al, 1983)
4. Gravity sliding (Kirkland and Anderson, 1970; Borns et al, 1983)

No real consensus has emerged from the various viewpoints. Currently, more detailed geochemical and petrological data are becoming available that may provide the answer.

Another crucial question is the timing of deformation. Several workers (Kirkland and Anderson, 1970; Anderson and Powers, 1978; Barrows, pers. comm., 1982) have inferred that the deformation has occurred during regional tilting over the last 30 my or that the deformation is ongoing because of deep dissolution or gravity inversion (halokinesis or gravity slide). On the other hand, C. L. Jones (1981) has suggested that deformation was limited to the Permian or Triassic, since Pliocene deposits such as the Ogallala are undeformed above DZ structures. Crucial to this argument is the question whether deformation in a layered evaporite sequence is always transmitted to overlying units.
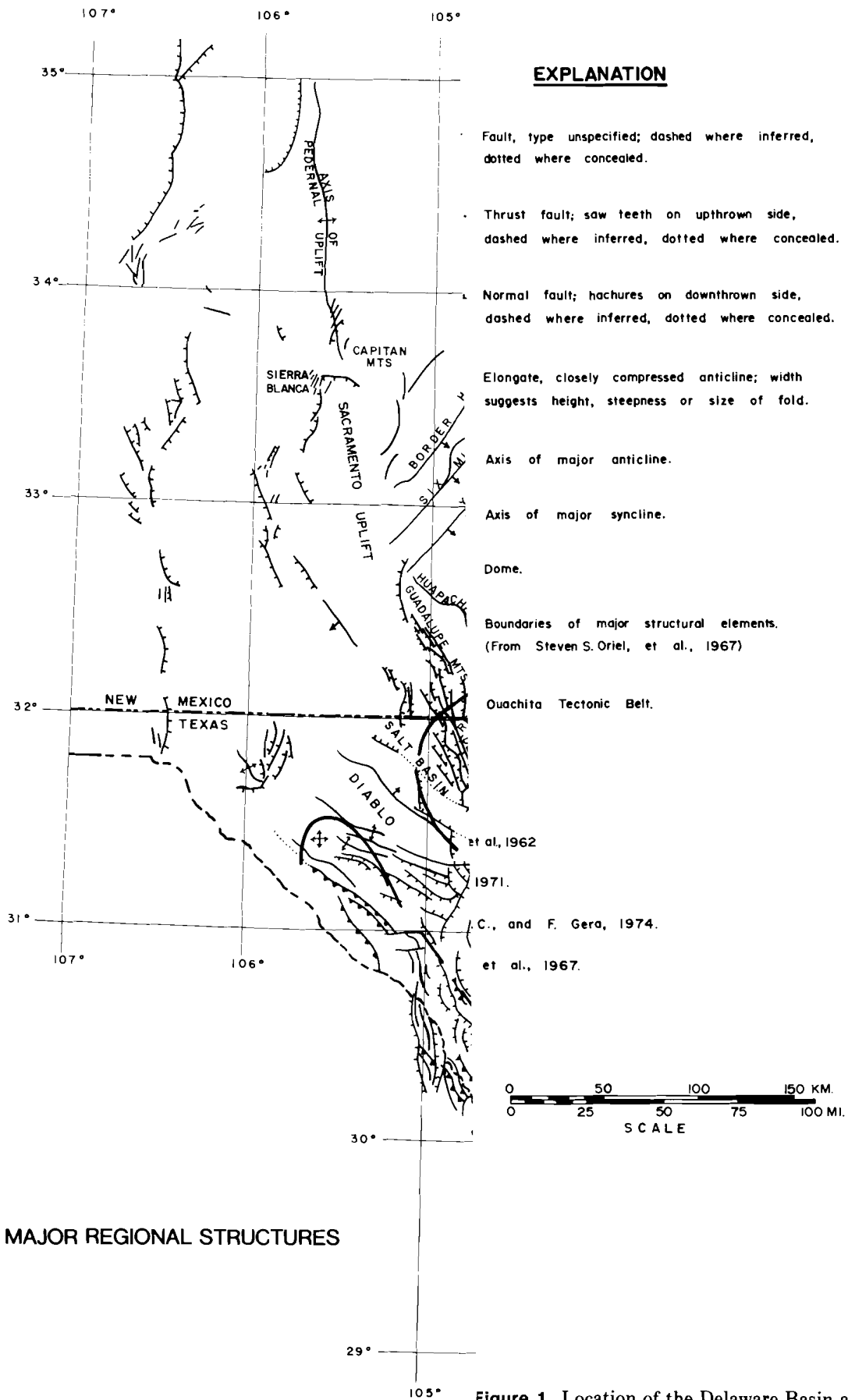
Figure 1. Location of the Delaware Basin and WIPP Site

Figure 2. Basin Stratigraphy

11
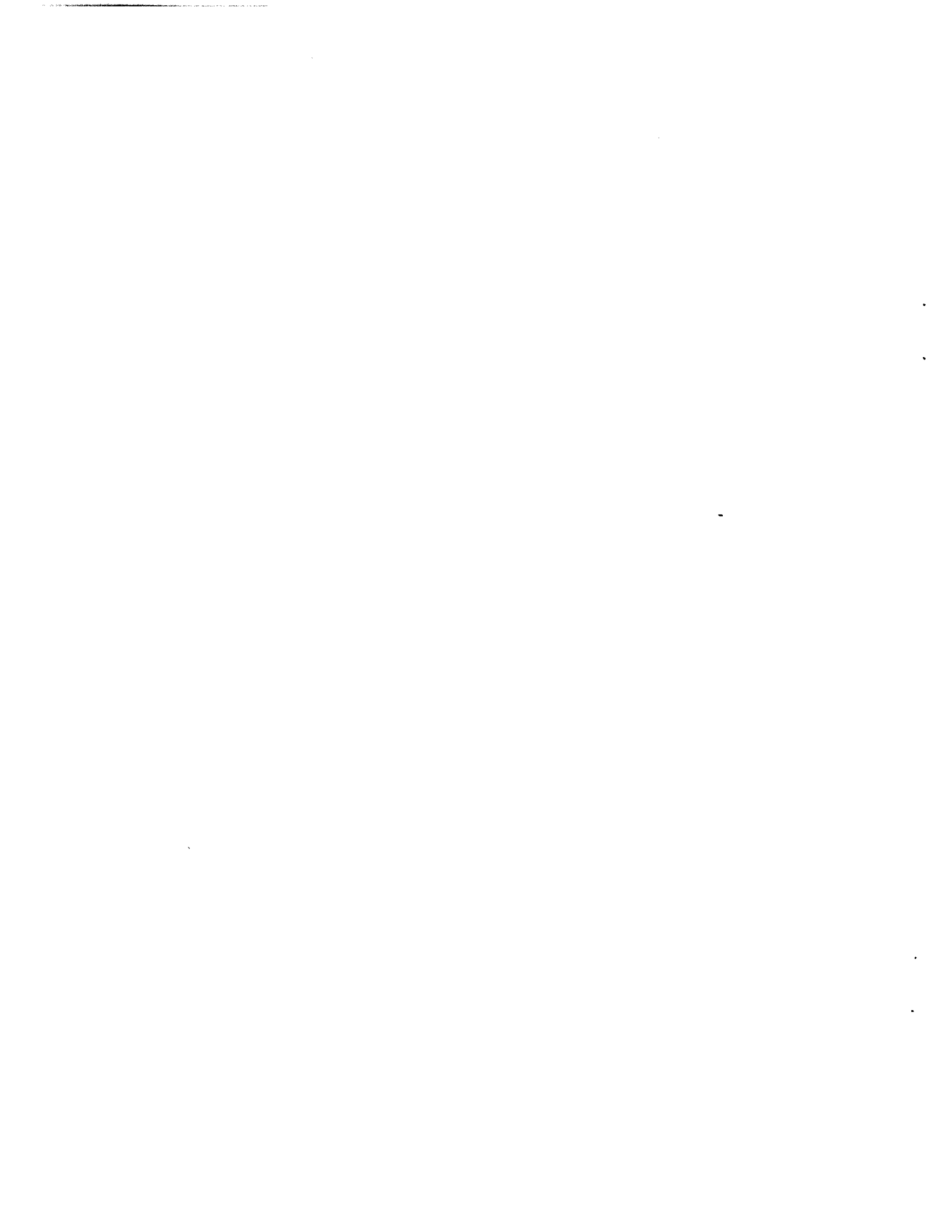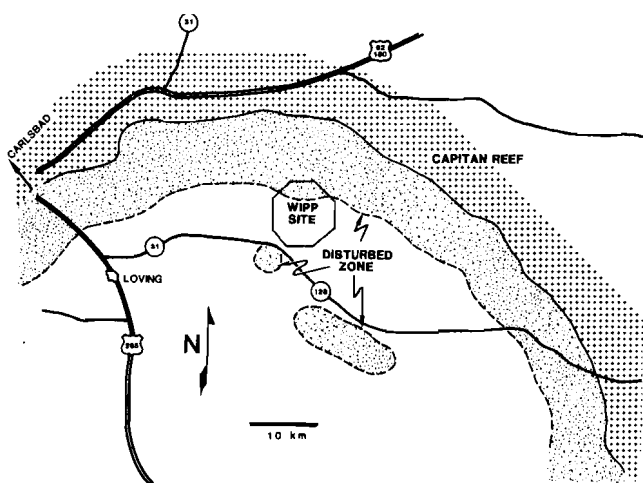
Figure 3. Location of WIPP Site and Areal Distribution of Disturbed Zone

The microscopic textures and petrofabrics of rocks from the DZ have heretofore received little attention. Callender and Ingwell (1978) reported on the structural petrology of experimentally deformed halite from the WIPP site. However, the experimental conditions extant probably cannot be extrapolated to the conditions during site deformation primarily because of the presence of natural fluids during deformation at the site. The study of petrofabrics generates insights into the mechanisms of deformation, relative movements, and possibly (but indirectly) the age.

1.1 Previous Work

Kirkland and Anderson (1970) reported the occurrence of microfolded evaporites from the Castile Formation. Their work was based on drill core, mine exposures, and limited outcrops in Eddy County, New Mexico, and Culberson and Winkler Counties, Texas. The microfolding was also apparently second-order to some larger scale warping (wavelength ~5 m). Kirkland and Anderson concluded that folding was tectonic in origin rather than syndepositional.

ERDA 6 was an early exploratory test hole in the Delaware Basin to evaluate a candidate site for a

nuclear-waste test facility (Jones, 1981). ERDA 6, however, revealed large-scale upward displacement in the Castile accompanied by thickening of Halite I (Anderson and Powers, 1978; Jones, 1981). Along with the large-scale deformation, complex meso- and microscopic folding similar to textures described earlier by Kirkland and Anderson (1970) was apparent in the drill core.

Seismic reflection data in the northern Delaware Basin are characterized by anomalous areas where reflector continuity is lost (Borns et al, 1983). Structure contours in this area indicate a terrain of anticlines and synclines (Snyder, 1982). Drill cores (WIPP 11, 12, and 13) from the anomalous areas also exhibit complex folding and extension structures similar to those encountered in ERDA 6. For the large part, the structures are restricted to the evaporite sequence without involvement of either the underlying Bell Canyon Formation or the overlying Dewey Lake Redbeds.

1.2 Method of Study

Core, which is housed in the WIPP Core Library, Carlsbad, New Mexico, was the source of samples used in this study. Oriented core was obtained from WIPP 12 and DOE 1. Samples were examined and described from drillholes ERDA 6, AEC 8, WIPP 11, 12, 13, and DOE 1 (see Figure 4). Core photographs, which are stored in the WIPP Central File from these holes and from ERDA 10, were also used in the reconnaissance of deformation structures. During mesoscopic study, intervals of interest were selected for microscopic study. These samples were slabbed into half-core barrels and moved to Albuquerque. Portions were cut and trimmed down to thin section size. These chips were impregnated with epoxy and mounted. Halite thin sections were cut with a Buehler wafer saw to reduce deformation caused by the sectioning process. Machine-ground specimens were finished by hand grinding. Microscopic description employed standard procedures. Petrofabric orientations were determined with a Leitz 5-axes universal stage following the methods of Emmons (1943) and Turner and Weiss (1963).
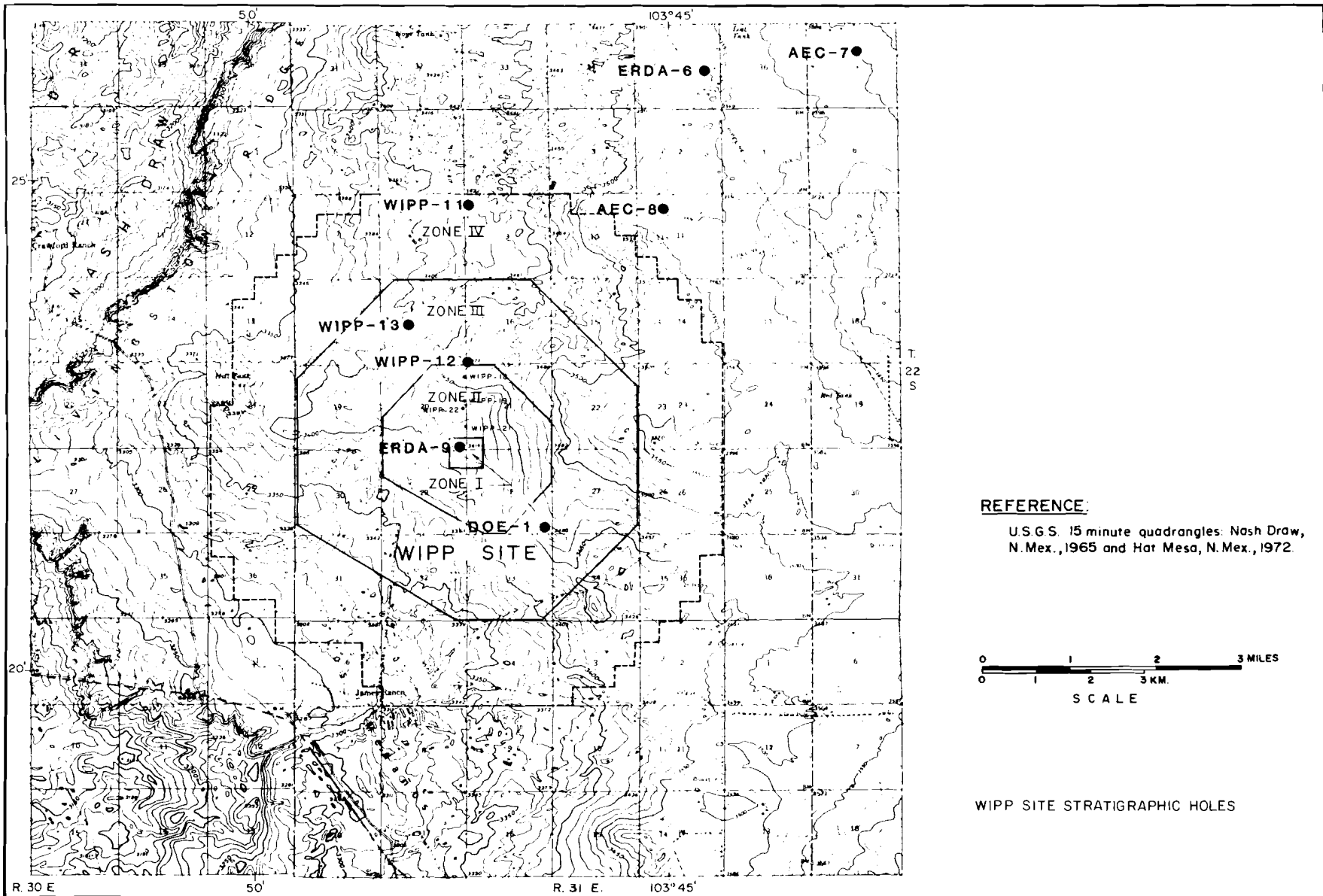
Figure 4. Drillhole Locations

REFERENCE:

U.S.G.S. 15 minute quadrangles: Nash Draw,
N.Mex.,1965 and Hat Mesa, N.Mex.,1972.

SCALE

WIPP SITE STRATIGRAPHIC HOLES

2. Mesoscopic Structures

Deformed evaporites display structures equivalent to metamorphic fabrics that have developed in silicate rocks (Balk, 1949 and 1953). Because of this similarity, evaporites have been used as field and experimental analogs for crustal deformation of silicate rocks. Hence, many techniques used in unraveling complex structural terrains apply to deformed evaporites, especially layered sequences such as in the Delaware Basin. The first step here is to characterize the styles of deformation. Such styles can be grouped together and used to fingerprint different stages of deformation.

These styles and related structures assist the structural geologist in four basic ways (Wilson, 1982): the visualization of larger scale structures; the indication of directions and sense of local movements; the indication of stress distribution; the placement within a time sequence of the different stages of deformation.

Table 1 shows the arrangement of deformation styles and stages in the northern Delaware Basin as inferred from the mesoscopic structures. In the following pages, each style and association is described in detail.

2.1 Syn- to Closely Postdepositional Structures

In Anhydrite I from both WIPP 13 and DOE 1, anhydrite laths grow upward from a flat surface and contort the overlying laminae (see Figure 5b and 5c). Elsewhere, isoclinal folds are exhibited in 1-cm layers. Such folds are isolated to the layer and commonly show an opposite sense of asymmetry relative to the more penetrative open-to-tight crenulation folds. Fold asymmetry and vergence are inferred senses of direction derived from this geometric relationship between a structure and the larger structure that contains it (Bell, 1981; Wilson, 1982, see Figure 6). In laminated anhydrite and carbonate units, some laminae have corrugated bottoms while their upper surface is flat. Dipping laminae (10° to 15°) are truncated along an unconformity at 1744 ft, ERDA 6. The restriction of these features to individual layers and relative incompetency of anhydrite-carbonate laminae at the time of deformation suggest that these structures formed locally during deposition or closely after deposition but before consolidation.

Table 1.   Stages of Deformation (Decreasing Relative Age Downward)

Stage	Process (What Occurred)*
Syndepositional to Closely Postdepositional	Isoclinal Folding 1. Isolated to single layers 2. Opposite sense of asymmetry relative to later stage folds More open Polyharmonic Crenulations (State Line Outcrop)

Tectonic	Laminated* Anhydrites	Halites	Infra-Cowden Cowden Anhydrite
Younger ↓	a. Shape fabric b. Open-to-tight asymmetric folding Microboudinage Crenulation cleavage c. Near-vertical fractures	a. Shape fabric b. Convolute Fold of anhydrite stringers c. Shear zones	b. Crenulation and zonal crenulation cleavage (stylolites)

Youngest Stage

*Syndepositional processes are independent of rock-type compared to tectonic processes, in which different processes occur in the individual rock-types during the same stage.
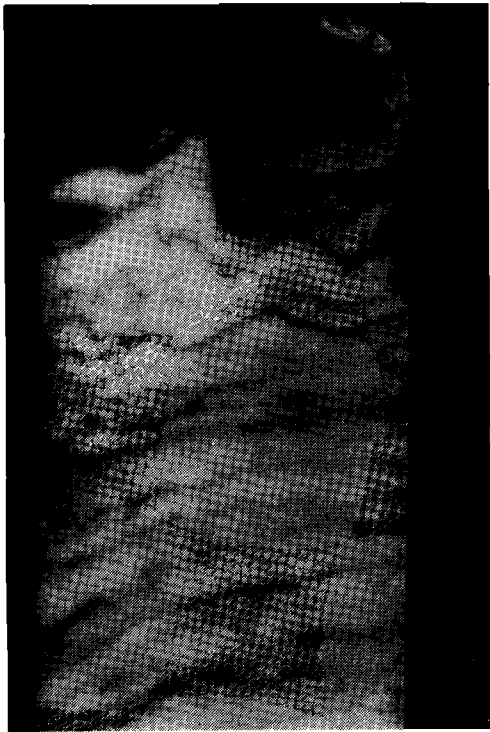
a. Deformed Coarse Laminated Anhydrite, ERDA 6, 2021 ft, Crenulation Microfolds, Incipient Crenulation Microfolds, Incipient Crenulation Cleavage
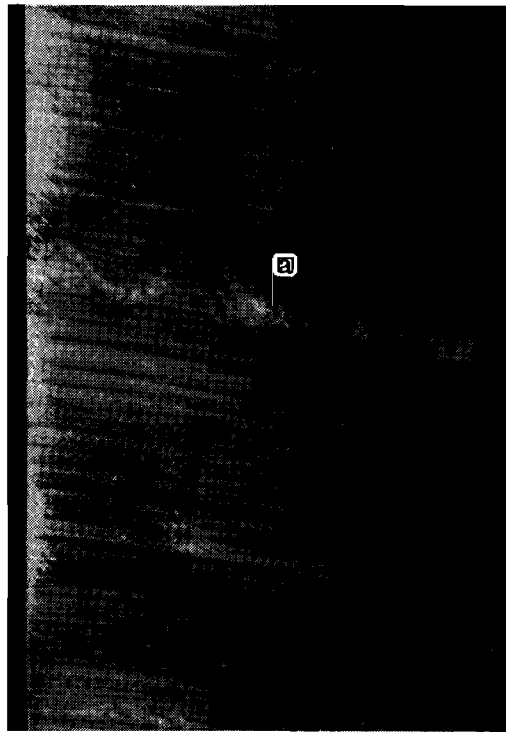
b. Relict Anhydrite (a) Needles (Syn- to Postdepositional) Growing Upward Into Anhydrite-Carbonate Laminae, WIPP 13, 3864 ft
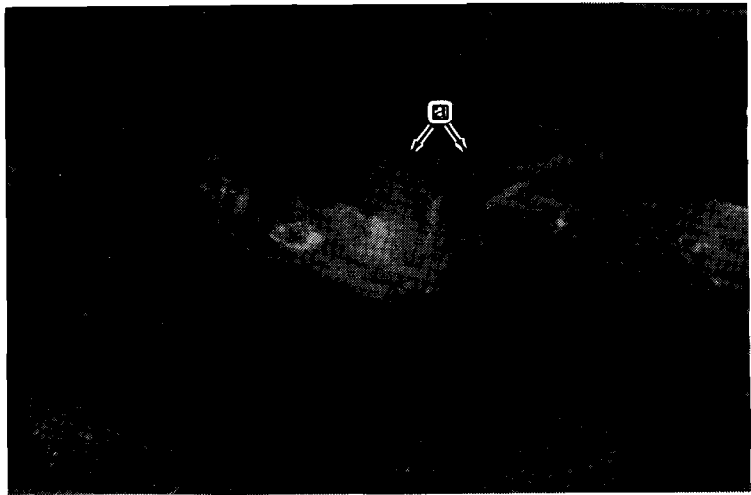
c. Detail of b, Anhydrite Needles (a)

Figure 5. Secondary and Primary Anhydrite Growth Structures
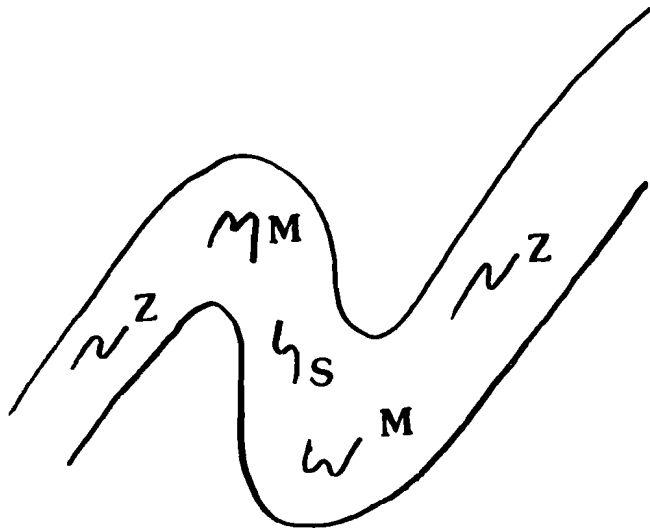
Figure 6. Second-Order Fold Symmetries and Asymmetries (symmetric M fold, asymmetric S and Z folds that have opposite senses of asymmetry)

At the State Line outcrop (Kirkland and Anderson, 1970), chaotic or disrupted layers up to 10 cm thick, are found sandwiched between undeformed laminae (see Figure 7). Some folds are abruptly truncated adjacent to their hinges. Another observation is of juxtaposed antiforms and synforms that share the same axial plane (Kirkland and Anderson, 1970, Figure 3b). Each layer needs to act independently of the over- and underlying units to accommodate the deformation. Also, the interlayer boundary must be a sliding surface. This independent behavior and the non-parallelism of folds from laminae to laminae suggest that these structures developed before consolidation. Similar folding has formed in the Zechstein salt deposits during redeposition (Schlager and Bolz, 1977). The deformation at the State Line outcrop is not to be taken as entirely syndepositional, for there exists a sizable component of microfolding that is penetrative and tectonic in origin (see Figure 7).

2.2 Shape Fabrics

A shape or dimensional fabric is defined as the tendency towards parallelism of one or more of the morphological axes as defined by inequidimensional units such as elongate, flaky, or prismatic crystals (Spry, 1969, p 207). In recrystallized halites, especially Halite II in the DZ, a foliation is defined by the planar arrangement of halite elongation axes (aspect ratios: 1:2). The foliation is parallel to the axial plane of folds exhibited by anhydrite stringers in the halites. The elongation of halite grains is commonly parallel and defines a lineation. Such fabrics are not mesoscopically as obvious in anhydrite laminae. Microscopically

(see Sec 3), anhydrites exhibit shape fabrics similar to those of halites.

2.3 Open-to-Tight Asymmetric Folding

As high in the section as the Cowden and Infra Cowden, a crenulation of the bedding surface has developed (see Figure 5a). Inclined to the bedding surface and parallel to the axial plane of the crenulation, a crenulation cleavage (stylolitic) is observed. Within the Castile proper, microfolding has a greater amplitude than in the beds above it (see Figures 8-13). Such microfolds are commonly asymmetric with a consistent sense of vergence at the core barrel scale. These asymmetric folds are most highly developed in the finely laminated (varved) anhydrite-carbonate units. When the core is broken along a foliation surface in a microfolded unit, the hinge lines of the folds mark a distinct lineation. Microscopic textures suggest that this fold stage developed after the initial shape fabric (see Sec 3).

The folding of anhydrite-carbonate laminae is not homogeneous. Layers, adjacent to microfolded layers, may be relatively undeformed. In larger amplitude microfolds, the laminae are discontinuous in the hinge zone, which imparts a blocky appearance to the fold. Halite and/or anhydrite veins commonly occur in the hinge zone parallel to the axial plane of the fold.

2.4 Convolute Folds of Anhydrite Stringers in Halites

Throughout Halites II and I, anhydrite stringers 0.5 to 1.0 cm wide occur. Such stringers can exhibit an asymmetric color banding with a basal red zone that is caused by the presence of carbonate. Idioblastic halite porphyroblasts are also common to the stringers. Convolute or ptygmatic folds of these stringers have developed (see Figures 13d and 14). Folds are tight to isoclinal with the axial plane parallel to the foliation imparted by the halite shape fabric. The fold hinges are at high angles to the shape fabric lineation of the halite. The asymmetric band coloration permits layers to be connected and, hence, helps to delineate larger scale folds (see Figure 14). Axial planes are predominantly subhorizontal. Some 20° inclinations are recorded, e.g., ERDA 6. The ptygmatic folding occurs in halites from relatively undisturbed areas encountered in holes such as AEC 7, 8, and DOE 1. Commonly, in the highly deformed regions, one limb of the fold has been displaced, and stringers developed pull-apart structures. In contrast, fold stringers in less deformed regions are largely continuous.

17
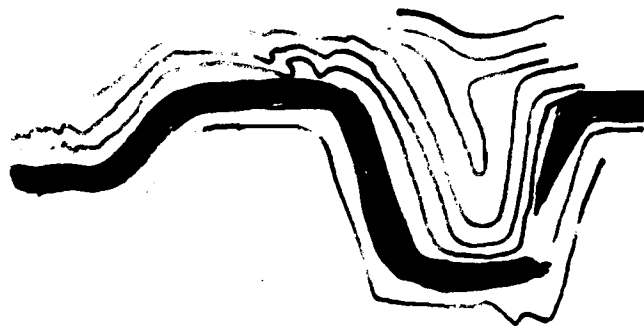
1 m

a. Box Fold With Disrupted Marker Layer
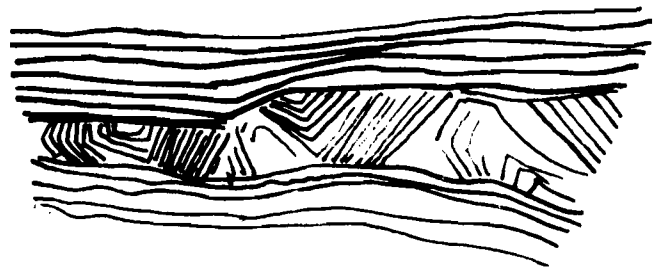
10 cm

b. Chaotic Layer Confined in Horizontal Layers
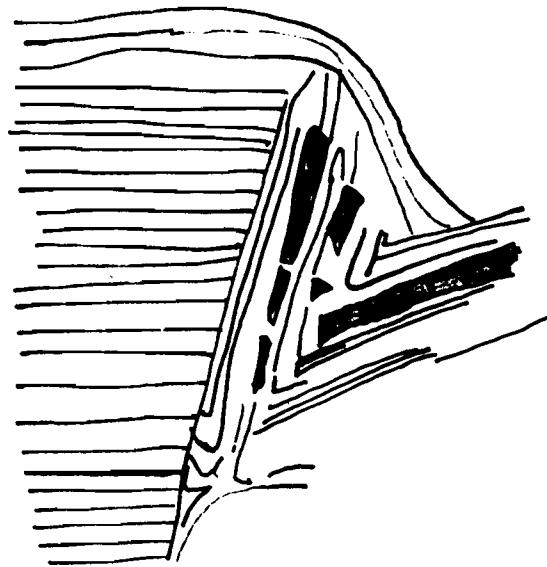
1 m

c. Blocky Fold Hinge, Sharp Truncations, Disrupted Marker Layers

Figure 7. Early-Stage (Syndepositional) Structures in Castile Anhydrite State Line Outcrop
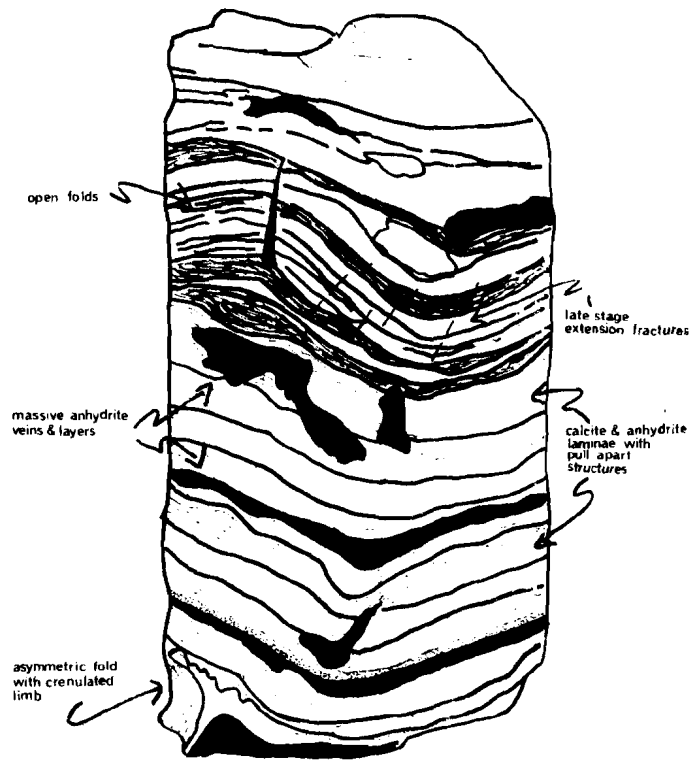
Figure 8. Deformation Styles in Laminated Carbonate Anhydrite Units in the Castile (WIPP 13, 3727 ft; width of slab 4 in.)
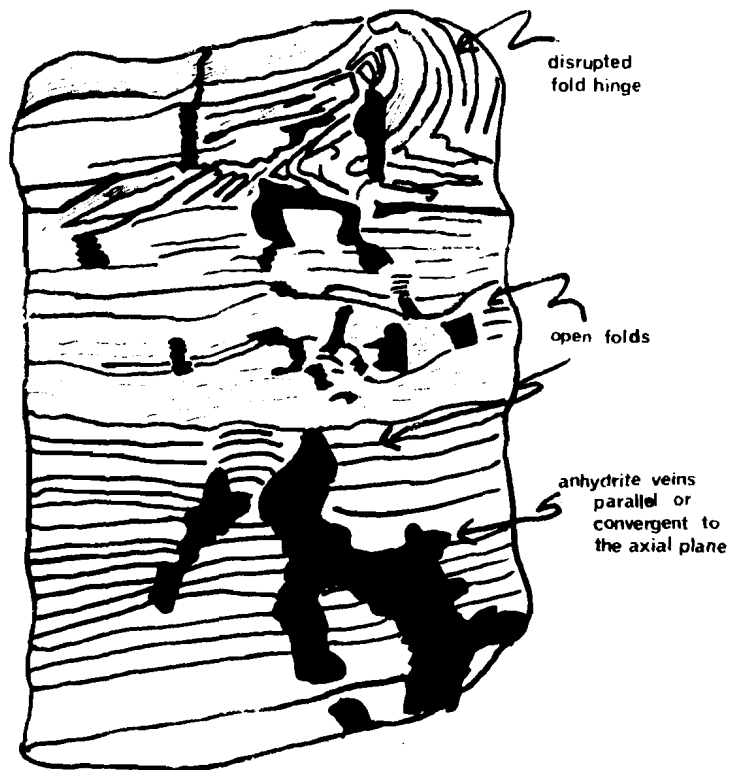
Figure 9. Deformation Styles in Laminated Carbonate Anhydrite Units in the Castile (WIPP 13, 3227 ft; width of slab 4 in.)
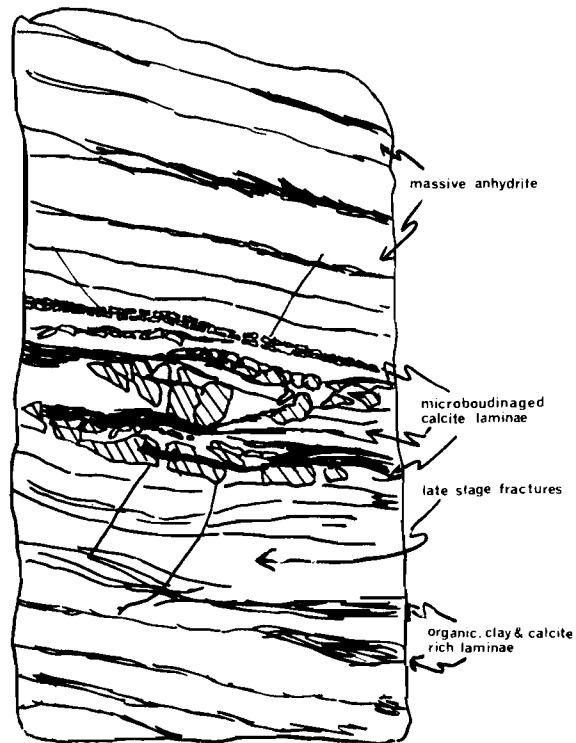
Figure 10. Deformation Styles in Laminated Carbonate Anhydrite Units in the Castile (WIPP 13, 3729 ft; width of slab 4 in.)
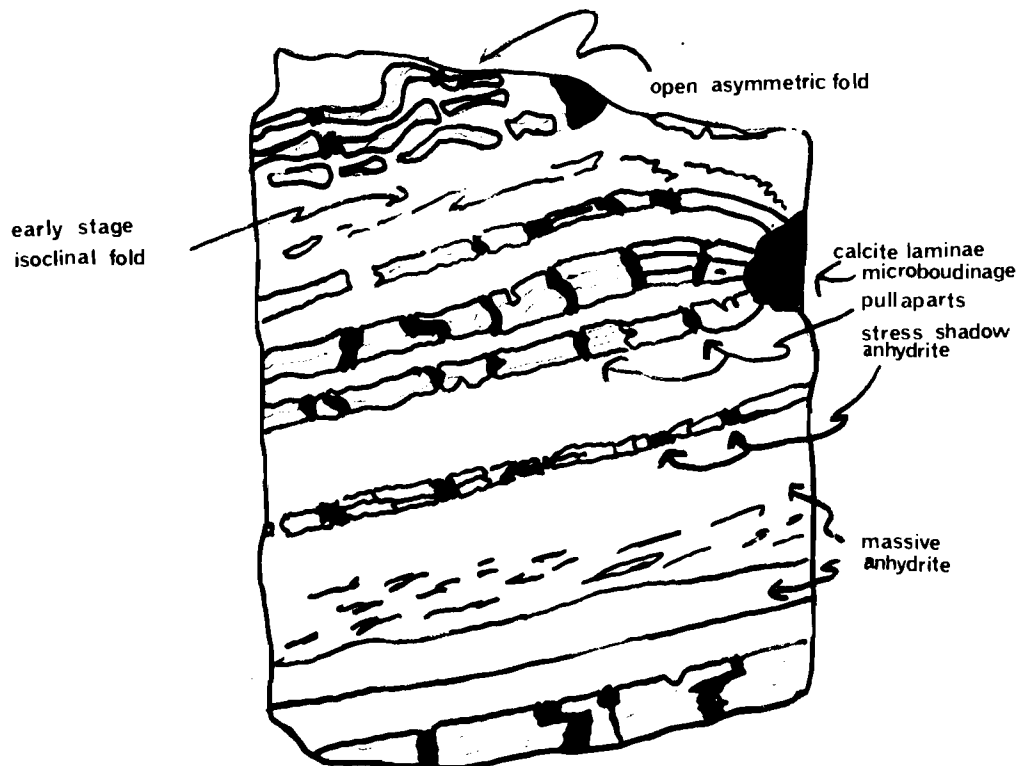
Figure 11. Deformation Styles in Laminated Carbonate Anhydrite Units in the Castile (WIPP 13, 3733 ft; width of slab 4 in.)

20

a. Open Fold With Compression (Microfolds) and Extension (Boudinage) Exhibited on Opposite Sides of Neutral Surface
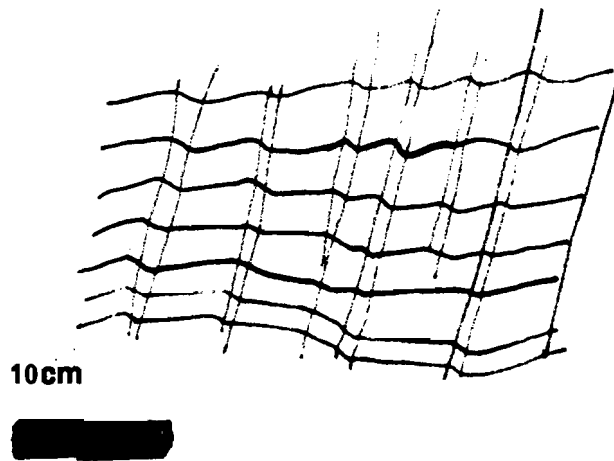
b. Asymmetric Microfolds and Crenulation Cleavage

Figure 12. Tectonic Deformation Structures in Castile Anhydrite State Line Outcrop

a. Complex Folding, Disrupted Layers, Anhydrite Recrystallization Patches and Stress Shadow Growth, ERDA 6, 2573 ft
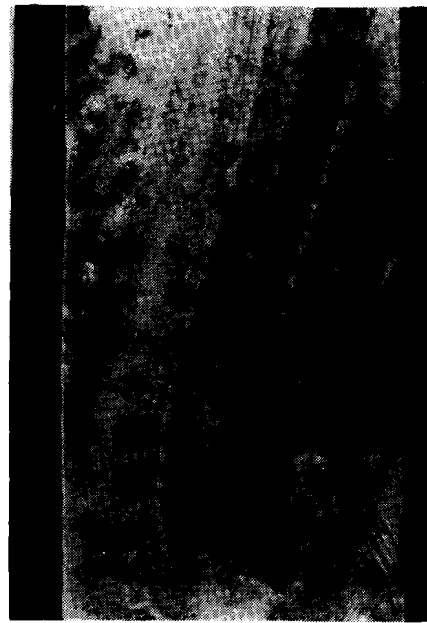
b. Tight Fold of Anhydrite-Carbonate Laminae, ERDA 6, 2574 ft

c. Boudinage of Carbonate Laminae With (a) Anhydrite Stress Shadow Growth, ERDA 6, 2699 ft
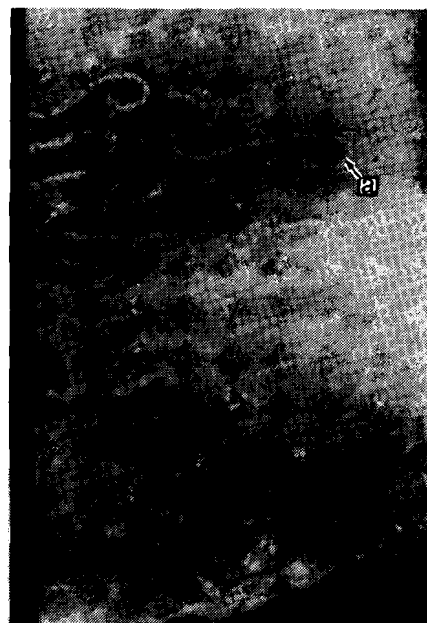
d. Convolute Isoclinal Folds of Anhydrite Stringers in Halite, 2775 ft; (a) shows anhydrite stringer

Figure 13. Deformation Structures From Castile Anhydrites and Halites (bars are 1 cm)

22

WIPP 11

283I

2774
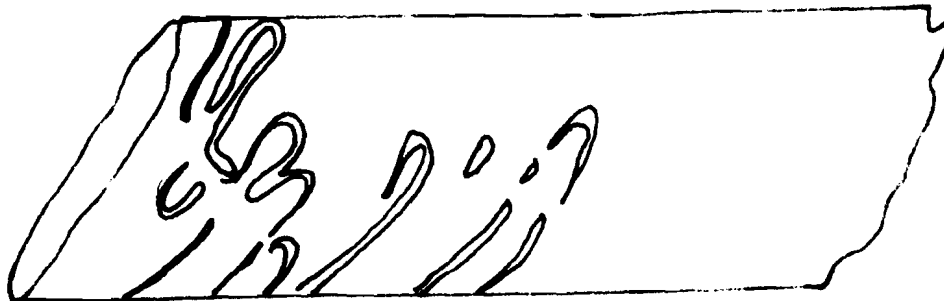
AEC 8

3734
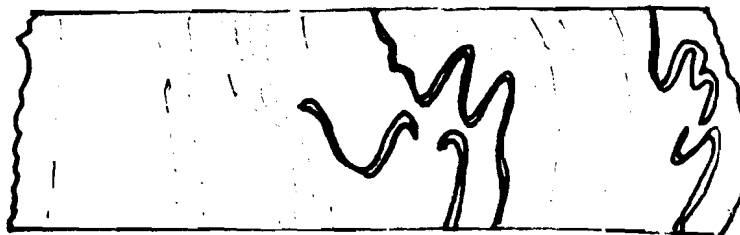
Figure 14. Convolute Folds of Anhydrite Stringers in Halite Units of the Castile

2.5 Relict Primary Halites

Some portions of the halite units in the Castile are relatively undeformed, e.g., Halite I in WIPP 12 and DOE 1. Such intervals are characterized by alternating layers of grey and clear halite, 5 to 10 cm in thickness. The alternation appears cyclic. Such layers are generally near-horizontal. Grain size is large (about 1 cm in diameter), and the core intercepts some single halite crystals greater in diameter than the core dimensions. Grain boundaries are relatively unsutured relative to boundaries in more deformed halites. Because of this looseness, the core is easily granulated. Anhydrite commonly forms an intergranular lacework in the cyclic halites.

2.6 Contacts Between Halite and Anhydrite Units of the Castile

Cores from holes bored in relatively undeformed and moderately deformed halites (AEC 7, 8, WIPP 12, and DOE 1), show that contacts between superimposed lithologic units are conformable. In contrast, other contacts observed in the Castile of ERDA 6 and WIPP 13 commonly crosscut the layered fabric of the anhydrites. Halite veins in the anhydrites occur adjacent to contacts, regardless of whether the contacts are conformable. These veins form either as infillings of vertical fractures (see Figure 15) or as irregular embayments into anhydrite (see Figure 16). In the embayments, halite replacement of anhydrite is commonly initiated along foliation planes. Larger halite patches contain clay residues that are planar and mark relict foliation surfaces inherited from the laminated anhydrite (see Figure 16c). Deformation of halite units is more distinct adjacent to contacts with anhydrite units. Near such contacts, ptygmatic folding of anhydrite stringers occurs, and the foliated shape fabric of halite grains has commonly developed.

2.7 Shear Zones Within Halites

Discrete subhorizontal zones, ~10 cm wide and subhorizontal, occur within both foliated halites and unrecrystallized primary halites, e.g., 3519 ft, 3645 ft (WIPP 12). These zones are characterized by a finer grain size than its host halite. When the host is a primary halite, the grain boundaries of the recrystallized shear zone are markedly tighter than those of the host. The shape fabric and boundaries of the shear zones can crosscut the bedding of the primary halite or the shape fabric of foliated halites outside the shear zone.

2.8 Boudinage

A boudinage structure consists of a segmented rock layer or vein of one type surrounded by a rock of a different type (Stromgard, 1973). The shape of boudins may be either rectangular, rhomboidal, or barrel-like. Between adjacent boudins, there generally occurs a pressure (stress) shadow. Such pressure shadows are either a secretionary type (filling of opening fracture) or replacement type (replacement of matrix).

Boudin structures are observed commonly in laminated anhydrite-carbonate units and in anhydrite stringers within halite units (see Figures 10, 11, 17, 18). Such structures were called "snap aparts" by Anderson and Powers (1978). Boudins in the laminated anhydrite-carbonate units exist at several scales; a sequence of boudinaged laminae (1 to 5 mm thick) are in turn boudinaged as a stack (5 cm thick; see Figure 8). Small-scale boudins are rectangular, with the carbonate bands the segmented competent rock type. Larger scaled boudins of multiple layers exhibit necking and are barrel-shaped. Secretionary-type pressure (stress) shadows have formed between segmented carbonate laminae. Anhydrite in-fills these shadows; halite may occur in larger scale shadow zones. Necking, if it occurs, is observed in the shadow zone or in the matrix (see Figure 16). Boudinage of anhydrite stringers in halite units is of the rectangular type.

2.9 Veins and Fractures

Veins and associated fractures developed in the anhydrites and carbonates through the main stage of deformation and into the waning stages. An irregular-to-planar vein network developed through the interconnection of stress shadows in pull-aparts (see Figures 8-11). Such veins are in-filled by anhydrite and, to a lesser degree, halite. Halite veins occur crosscutting or along the foliation of laminated anhydrite (see Figures 15 and 16). In such veins, the halite has replaced portions of the laminated anhydrite, but a clay-rich residue remains in the halite and records the foliation of the laminated anhydrite that was replaced. These halite veins are also found as en echelon structure.

ERDA 6

2076
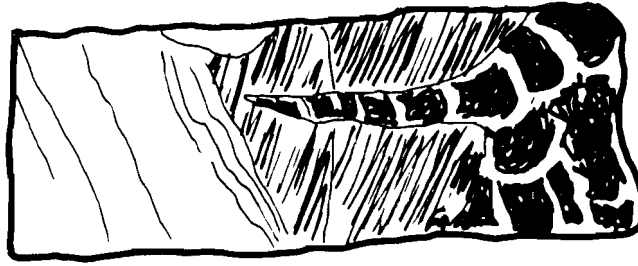
a. Near-Vertical Vein of Halite Extending Into Massive (Cross-Hatched) and Layer Anhydrite From Massive Halite at Contact

2168
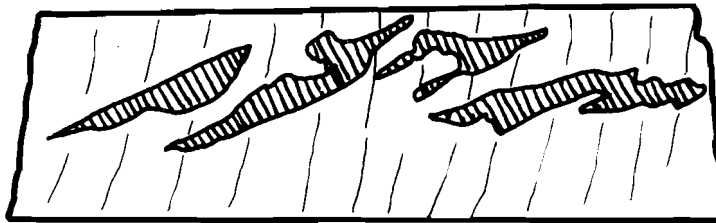
b. En Echelon Halite Veins (Cross-Hatched) in Laminated Anhydrite

WIPP 13

3523
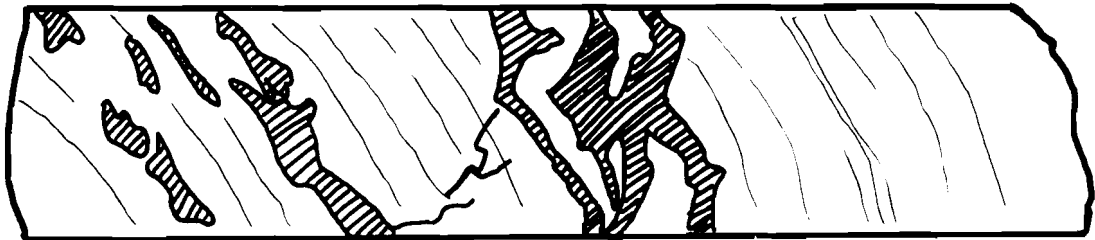
c. Crosscutting and Layer-Parallel Halite Veins (Cross-Hatched) in Laminate Anhydrite

WIPP 12

3062
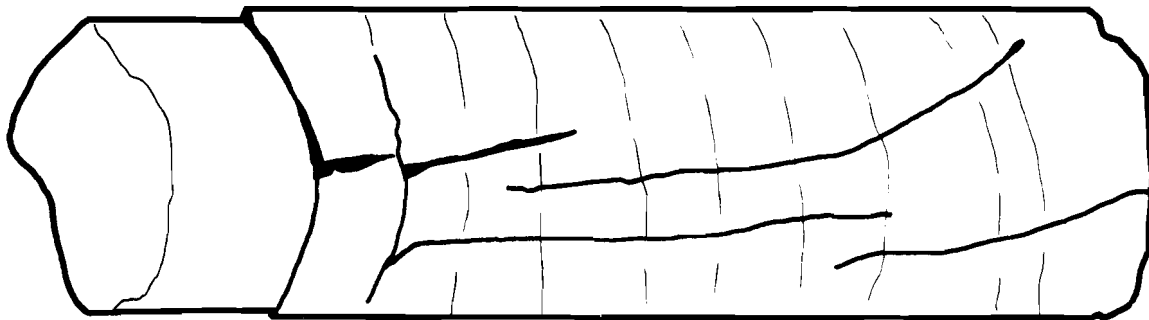
d. Halite-Filled Fractures at HII-AIII Contact

Figure 15. Vein Structures in the Castile and Infra Cowden Anhydrites

ERDA 6
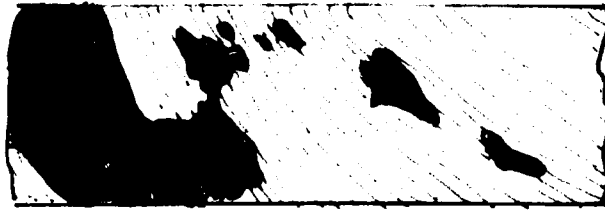
2733

a. Halite Vein (Solid) Embaying and Replacing Laminated Anhydrite

2733

b. Halite (Solid) Replacing Anhydrite Along Foliation Plane
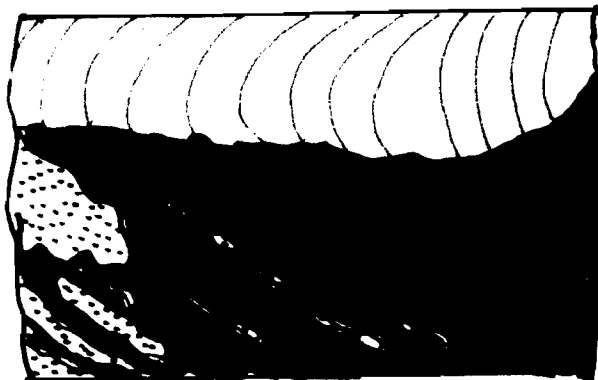
2732

c. Halite (Solid) Replacing Anhydrite, Clay Residues (Stipple) Records Foliation (Ruled) Inherited From Replaced Anhydrite

Figure 16. Vein Structures in Anhydrites From ERDA 6

26

WIPP 11   3505

a. Boudinage of Carbonate Layer in Laminated Anhydrite, Stress Shadow (Black) Growth is Anhydrite, Necking of Stress Shadow and Matrix

WIPP 12   3055

b. Boudinage of Anhydrite Stringer in Halite

3054
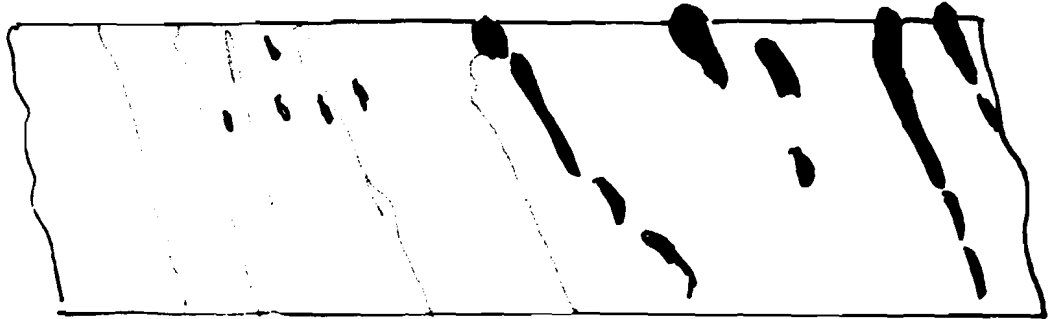
c. Boudinage of Anhydrite Stringer in Halite

WIPP 13

3728

d. Comminuted Carbonate Layer in Anhydrite Matrix, Late-Stage Fractures Emanate From Zone Into Bounding Anhydrite

Figure 17. Boudinage Structures

27
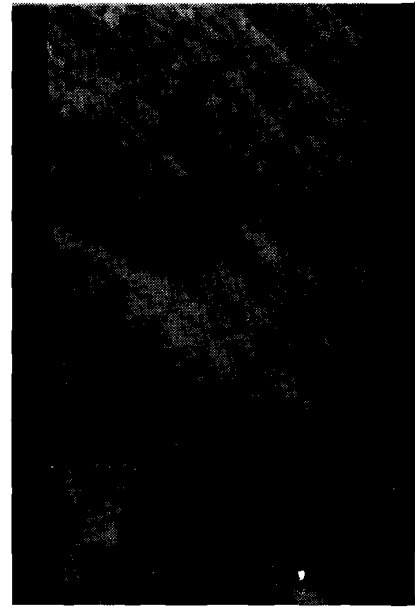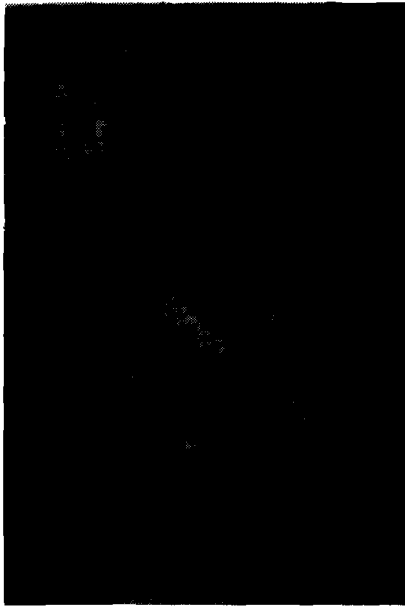
a. & b. Barrel-Shaped Boudins in Carbonate Layers, Anhydrite and Halite Stress shadows, ERDA 6, 2561 ft
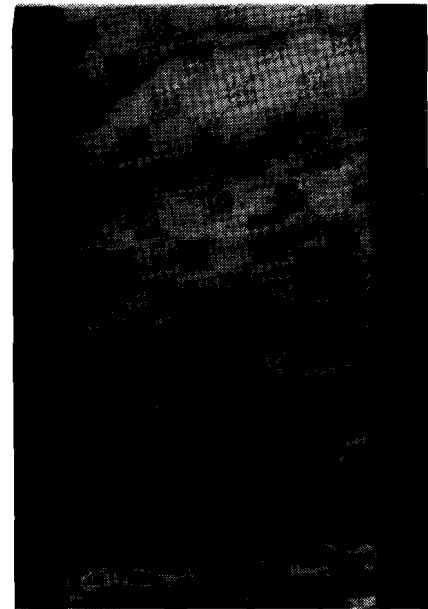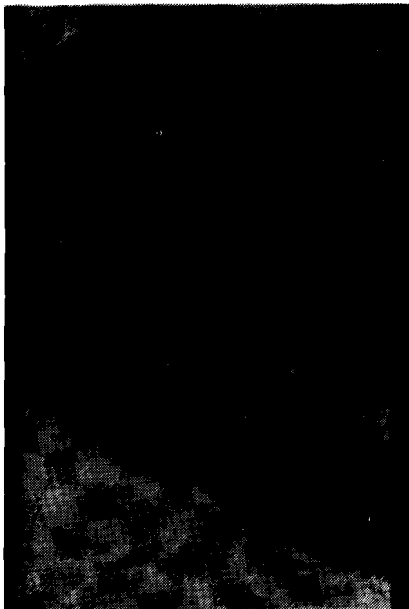
c. Comminuted and Rectangular Boudins of Carbonate Layer, Late-Stage High-Angle Fractures, WIPP 13, 3593 ft

d. Comminuted Carbonate Layer ERDA 6, 2021 ft

Figure 18. Boudinage Structures in Laminated Anhydrite-Carbonate Units in the Castile (bars are 1 cm)

Near-vertical fractures are observed crossing laminated anhydrites. Such fractures are of interest since they are associated with the brine occurrence at WIPP 12. In the core, these fractures are seldom greater than 2 mm wide, although 1-cm-dia gypsum crystals were found in a wide vug associated with a fracture at 2944.3 ft from WIPP 12. Fractures may be open or infilled by halite, anhydrite, and/or gypsum. Several fracture sets of different orientation have formed and are observed to intersect, e.g., WIPP 12, 3051 ft. Near the contact with Halite II at WIPP 12, the vertical fractures widen to 1 cm and are in-filled with halite (see Figure 19).

These high-angle fractures crosscut deformation structures such as anhydrite foliation and microfolds. Hence, such fractures are a late-stage manifestation in deformed anhydrites. These fractures are related to the brine reservoirs encountered in the DZ. The orientation of the fractures is an important consideration in characterizing the brine reservoirs.

In discussing the orientation of the fractures, Popielak et al (1982) have chosen to use teleseis viewer data. Their choice was based on the orientation of fractures, which the teleseis viewer shows as parallel and less random than the orientation pattern created with the oriented-core data. This conclusion was based on the assumption that the fractures should be parallel; however, in the domal structure such as at WIPP 12, radial and orthogonal fracture sets may develop. Some fractures observed in the WIPP 12 core, e.g., 3051.5, do intersect at a high angle. In this report, we have chosen to use the oriented-core data. As seen in Figure 20, a consistent orientation of lineations and poles-to-S-surfaces is displayed through the use of data from different oriented-core, which in turn implies a core-to-core consistency in orientation. The reader must be wary that the different interpretations of the orientation data cannot be reconciled at this time.

2.10 Oriented-Core Studies

Oriented core was obtained from WIPP 12 and DOE 1. For graphical analyses, limitations are imposed on the interpretation by the low number of readings (≤ 50) from each hole. Also, a discrepancy exists between teleseis viewer orientations and the oriented core. However, the consistency of fabric orientation in the three oriented barrels from WIPP 12 suggests the internal reliability of these data.

Graphical analyses of WIPP 12 orientation data indicates that fractures are near-vertical, but do not have a preferred orientation (see Figure 20). S-poles delineate a partial girdle that trends NE-SW. This girdle would indicate the existence of a fold axis, running NW-SE. Such an axis corresponds to the cluster of lineations in the NE. This cluster is slightly NE of the expected axes; hence, there may be a rotation of this cluster to the NE into a movement direction.

The halites from DOE 1 are weakly deformed. S-poles produce a diffuse pattern with no suggestion of an oriented fabric (see Figure 21). Also, no apparent concentration of lineations exists.

2.11 Discussion: Mesoscopic Structures

2.11.1 Areal and Depth Distribution of Deformation

Figures 22, 23, 24, and 25 diagrammatically display the distribution of deformation in the holes studied. Inclined bedding and crenulation folds are observed as high as the lower Salado in ERDA 6 and WIPP 13. Such deformation becomes more distinct in the Infra Cowden. Even in relatively undisturbed areas encountered in holes (e.g., AEC 7, 8, ERDA 10, DOE 1), folded anhydrite stringers in Halite I or II suggest some salt movement. Within a single hole or from hole to hole, the intensity of deformation between Halite I and II varies. Generally, Halite II exhibits more recrystallization and folding than does Halite I. Exceptions are the relatively undisturbed areas encountered in AEC 8, where the folded anhydrite stringers are found in Halite I. In highly deformed regions, cyclic primary halite is preserved in Halite I. Still, shear and folded zones locally cross these primary halites.

The correlation of thickening or thinning of Halite I or II to the intensity of deformation is not defined. In part, this is due to incomplete sampling of the units in question, such as at ERDA 6. For example, in WIPP 11, Halite II is apparently thickened and exhibits some of the most penetrative deformation observed. However, at WIPP 12, Halite I is apparently thickened but preserves primary halite bedding, although there are discrete zones of deformation present. Thinned halite units in WIPP 13 show extensive recrystallization. Hence, deformation structures are related to salt movement, but the actual connection is as yet unclear.

WIPP 12

3198
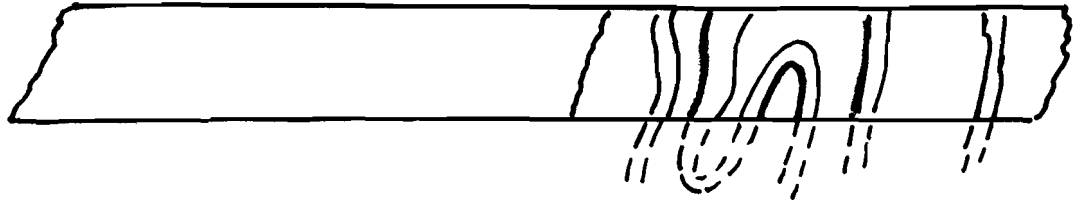
3105
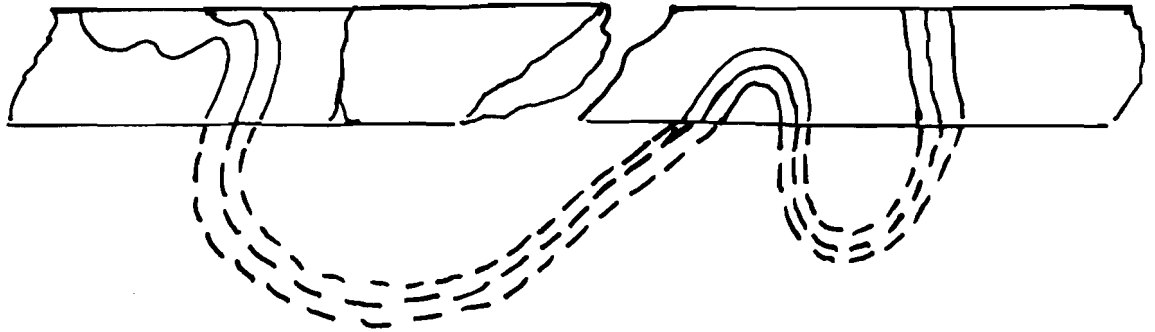
3107
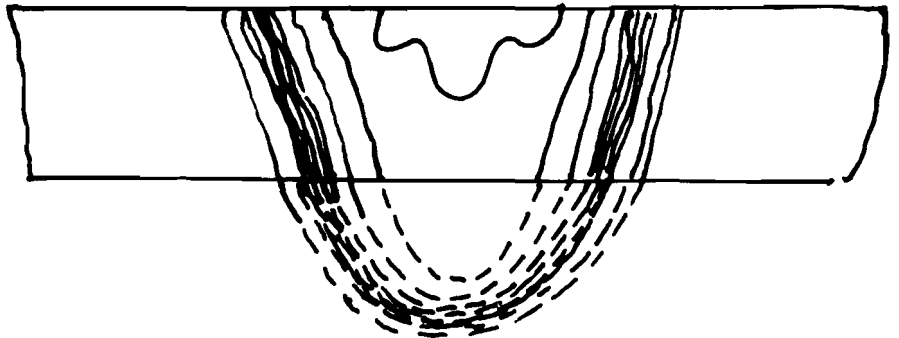
AEC 8

3726
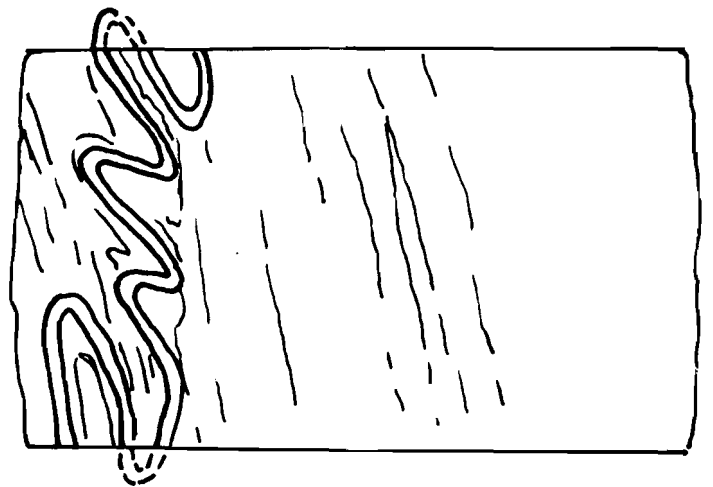
Figure 19. Folded Anhydrite Stringer in Halite Units of Castile, Where Distinctive Markers Can Be Traced and Which Define Fold Closure
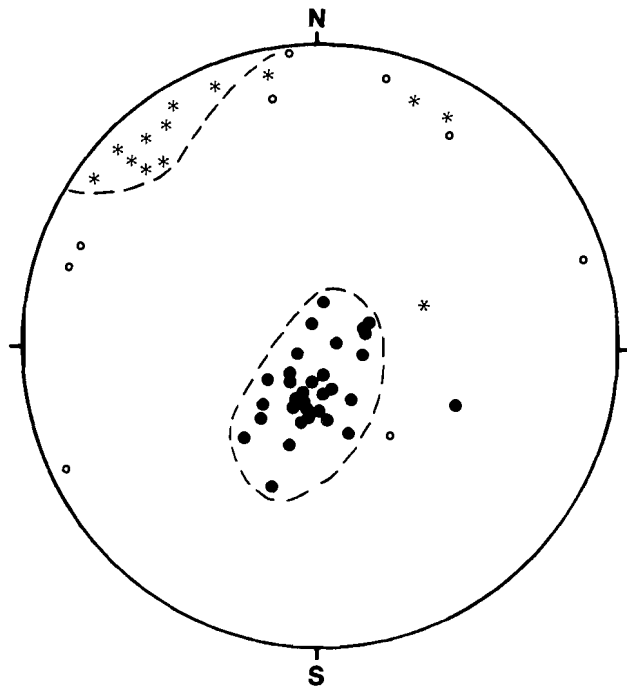
Figure 20. Linear and Planar Structures, WIPP 12 (• Normal to S-Surface; o Normal to Fracture Surface; * Fold Hinge Lineation)
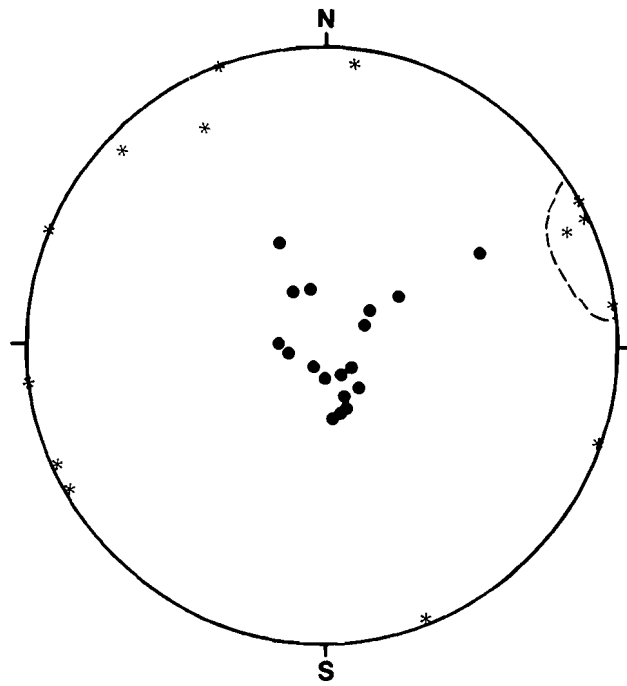
Figure 21. Linear and Planar Structures, DOE 1

ERDA 6

2000

unconformable contact, dipping beds, crenulated anhydrite, folded nodular anhydrite

dipping beds, crenulated anhydrite, halite shape fabric, halite veins, dipping beds

discordant contact, foliated halite, halite veins, folded anhydrite stringers

inhomogeneous halite fabric boudinage

folded anhydrite stringers, boudinage

crosscutting halite veins at contact between laminated anhydrite and halite (whether HII or HI uncertain)

3000

AEC 7

3000 AIII

relatively undeformed anhydrite stringers

HII

AII

steep dips

folded anhydrite, halite veins

4000 HI

crenulated carbonate layers

AI

folded carbonate laminae, conformable contact

Figure 22. Hole-to-Hole Deformation Features, ERDA 6 and AEC 7 (depths in ft below ground level; for location of holes, see Figure 4)

32
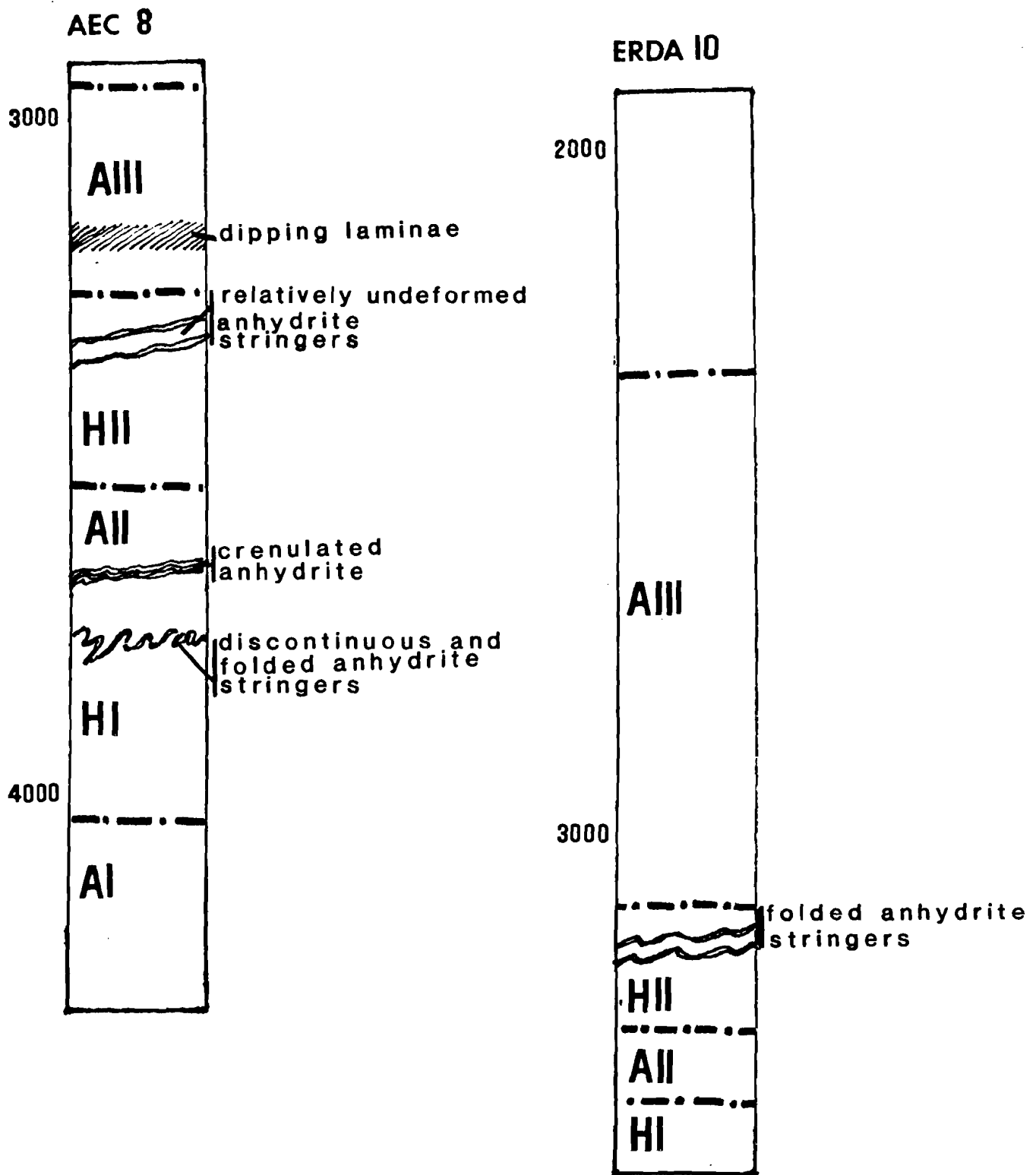
Figure 23. Hole-to-Hole Deformation Features, AEC 8 and ERDA 10 (depths in ft below ground level; for location of holes, see Figure 4)
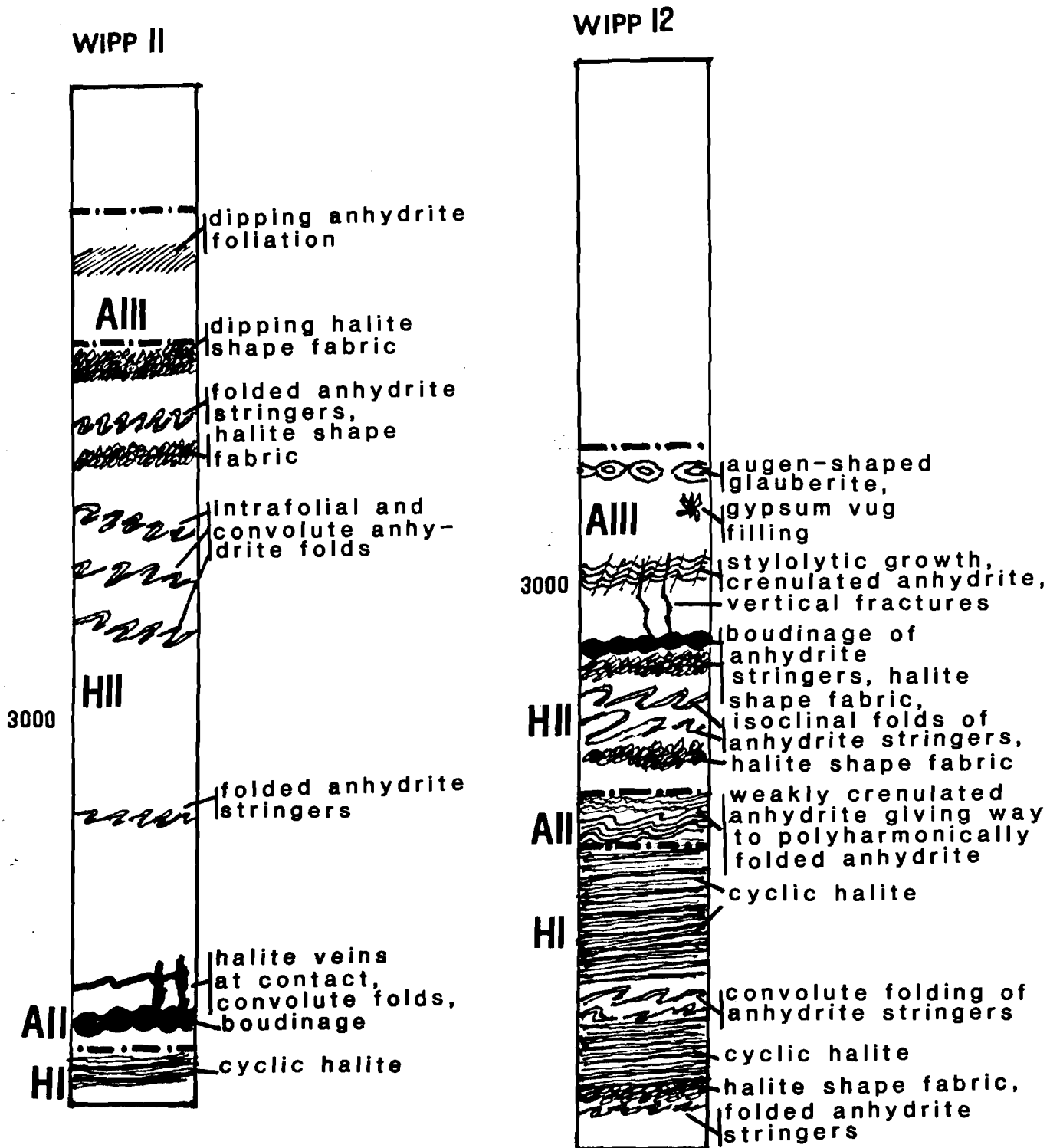
Figure 24. Hole-to-Hole Deformation Features, WIPP 11 and WIPP 12 (depths in ft below ground level; for location of holes, see Figure 4)

WIPP 13

crenulation cleavage

dipping halite
shape fabric
convolute anhydrite
stringers

folded nodular
anhydrite,
coarser grained
halite fabric,
dipping and micro-
folded anhydrite
and carbonate
laminae

3000

crenulation cleavage,

AIII

crenulation cleavage

halite vein work
parallel to
anhydrite laminae,
halite shape fabric

HII

AII

asymmetric folds,
blocky hinges,
halite veins,
boudinage
crosscutting
halite-anhydrite
contact

HI

AI

convolute folds
in anhydrite laminae

4000

Figure 25. Hole-to-Hole Deformation Features, WIPP 13
(depths in ft below ground level; for location of hole, see Figure 4)

2.11.2 Deformation Stages

In the northern Delaware Basin, deformation has been episodic and progressive. Early-stage syndepositional folding is seen in layer-bound isoclinal folding and crenulations. Such features may have developed through soft-sediment deformation on inclined surfaces and redeposition (Parea and Ricci-Lucchi, 1972). Progressive tectonic deformation initiated with flattening of original grains, which formed foliated-shape fabrics in anhydrites and halites. This fabric was folded when asymmetric open folds developed along with boudinage of competent carbonate laminae. The last stages of deformation were marked by the formation of near-vertical fractures in competent anhydrite-carbonate laminae.

2.11.3 Fluids Associated With Deformation

Vein systems developed syn- to postkinematically. Stress shadows and halite replacement zones in anhydrites suggest a process of solution and redeposition. The presence of fluid during deformation is inferred from such observations. This fluid is active in the sense that it migrates and is involved in the mass transfer during deformation.

2.11.4 Effects of Deformation

The extent of deformation is not homogeneous with hole-to-hole correlation nor within a single hole.

Cyclic primary halites are preserved in Halite I of deformed regions, e.g., WIPP 11 and 12. Strain may be accommodated along discrete shear zones in halites. With deformation confined to these zones, delicate primary structures such as hopper crystals are preserved. Deformation features are more extensive in Anhydrite II and Halite II than in other units of the Castile. Weakly deformed Anhydrite III lamina are characterized by inclined bedding, veins, and near-vertical fractures.

Halites, which recrystallized during deformation, appear to have more sutured (tighter) grain boundaries and to have experienced a reduction in grain size. Also, the intergranular anhydrite lacework, present in undeformed halite, is absent. Such observations suggest reorganization of the grain boundaries and, in turn, some destruction of porosity during deformation.

2.11.5 Directions of Movement

The minimal amount of reliable orientation data from holes in the DZ does not permit a determination of directions of elongation and shortening (see Sec 2.9). The near-horizontal orientation of axial planes from convolute and isoclinal folds in halite suggests a strong horizontal component of flow in the halite units. But the axes of folds show minimal rotation into a possible elongation direction, as inferred from the shape fabric.

3. Microscopic Structures

As with mesoscopic fabrics, microfabrics of evaporites can be indistinguishable from metamorphic tectonites (Schwerdtner, 1970). Anhydrite and halite deformation mechanisms have been studied in detail (Carter and Heard, 1970; Guillopé and Poirier, 1979; Heard, 1972; Muller and Briegel, 1978; Muller et al, 1981; Wawersik and Hannum, 1980). In part because of the difficulty in thin-sectioning, naturally deformed halites seldom have their microscopic textures described. Callender and Ingwell (1978) have studied microtextures from experimentally deformed halite. Anhydrites, on the other hand, have received more attention (Schwerdtner, 1970; Muller et al, 1981).

Again, the similarity of evaporite tectonites and metamorphic tectonites in silicate rocks suggests that standard textural analysis as developed for silicates is applicable to evaporites.

3.1 Deformation Mechanisms

The following deformation mechanisms may be active on the microscopic scale in geologic materials.

- Cataclasis (fracturing, frictional sliding)
- Dislocation mechanisms (dislocation glide, dislocation creep, steady-state flow processes)
- Shape changes of individual grains by grain boundary or through-the-grain (volume) diffusion, with a component of grain boundary sliding (Coble creep, Nabarro-Herring creep, superplastic flow)
- Pressure solution that is geometrically equivalent to the diffusion process above

The effectiveness of an individual mechanism is a function of several parameters: temperature (T); stress (deviatoric or differential, σ); strain rate ($\dot{\xi}$); viscosity (η); grain size; the presence or absence of an intergranular fluid. In experiments on the deformation of natural anhydrites, Muller et al (1981) found that at geologically reasonable strain rates, 10^{-10} to 10^{-14} s^{-1}, drastic strength reduction occurred at a threshold of 180°C to 200°C. Microscopically, samples deformed at lower temperatures exhibited undulatory extinction and, therefore, the deformation was some combination of cataclasis and ductile behavior. At higher temperatures twinning became the dominant mechanism. As deformation increased, lattice

reorientation occurred by shear twinning and twin boundary migration. Again, as temperature increased, dynamic recrystallization proceeded. Sutured grain boundaries were observed and suggest that grain boundary migration occurred. Generally, Muller et al (1981) found that intracrystalline glide and twinning were the major deformation mechanisms active during the steady-state flow.

The mechanical behavior of halite has been investigated for nearly 100 yr. A review of previous work up until 1970 appears in Carter and Heard (1970). Experimental studies have been done both on polycrystalline aggregates (Heard, 1972; Wawersik and Hannum, 1980) and single crystals (Carter and Heard, 1970). A common form of mechanical behavior in halite is translation gliding on {110}, {111}, and {001}; which of these glide systems is dominant depends on the crystal orientation relative to the principal stress axis, as well as temperature and stress. In experimentally deformed samples from ERDA 7 and 9, Callendar and Ingwell (1978) observed intercrystalline rotation, followed by translation gliding.

In halites, strain rate and viscosity are related and dependent on the differential stress in the following ways: the strain rate is proportional to the differential stress raised to a power; viscosity is a function of differential stress (σ) and strain rate ($\dot{\xi}$), $\eta = \alpha \cdot \sigma/\dot{\xi}$ where α is a constant (Heard, 1972). The effect of rising temperature on the mechanical behavior of halite can be pronounced. At low T and P, Wawersik and Hannum (1980) noted that polycrystalline halite exhibited dilatancy and loss of load-bearing capacity. The development of microfractures governs this dilatancy. At low to intermediate temperatures (up to 300°C) and high stresses, the deformation of halite is controlled by slip systems, such as {110}, {1$\bar{1}$0}, which are dependent on crystal orientation (Heard, 1972). Guillopé and Poirier (1979) experimented with single crystals of pure and impure halite through a temperature range of 250°C to 790°C. Dynamic recrystallization occurred at the lower experimental temperatures and stresses through subgrain rotation without grain boundary migration. At higher temperatures and stresses, recrystallation resulted from migration of high-angle grain boundaries. Strain hardening, which is related to the interaction and piling up of dislocations at a barrier, occurs in association with the lower

Org.	Bldg.	Name	Rec'd by	Org.	Bldg.	Name	Rec'd by